Early Collision and Fragmentation Detection of Space Objects without Orbit Determination

Lyndy E. Axon*

This paper demonstrates that from using the hypothesized constraint of the admissible regions it is possible to determine if a combination of new uncorrelated debris objects have a common origin that also intersects with a known catalog object orbit, thus indicating a collision or fragmentation has occurred. Admissible region methods are used to bound the feasible orbit solutions of multiple observations using constraints on energy and radius of periapsis, propagating them to a common epoch in the past, and using sequential quadratic programming optimization to find a set of solution states that minimize the Euclidean distance between the observations at that time. If this given this set of solutions intersects with a catalog object orbit, then that object is the probabilistic source of the debris objects. This proposed method is demonstrated on an example of a low-earth object observation.

I. Introduction

A problem of constant concern for the future of space operations, especially as massive thousand-satellite constellations are in the design phase, is the tracking, orbit determination, and cataloging of all space objects in orbit around Earth. The U.S. Air Force Space command utilizes the Space Surveillance Network (SSN) to make approximately 80,000 daily observations to track which make an estimated population of over 300,000 objects with a diameter of over 1 cm, 17,000 known catalog objects greater than 10 cm in diameter, and 1300 active satellites[1,2].[3] In over 50 years of space missions, over 5000 satellites have gone into orbit, of which less than 1300 are still operational today.[4] Many of the remaining satellites have deorbited successfully, or were put into designated storage orbits prior to end-of-life, however, a large number of them are dormant orbiting the Earth.[5] In addition to defunct satellites, debris from collisions, fragmentations, and launch litter the operational orbit environments from LEO to GEO. Not all the SSN's daily observations, or uncorrelated tracks, can be used to create actionable information.

Extracting actionable information from an initial UCT, is not a simple task, for with a single UCT it is not possible to uniquely identify the state of the object, or how useful it would be to immediately prioritize additional observations.[3] On a daily basis, thousands observations of space objects from the SSN take place over short time periods and do not posses enough observation data geometric diversity to initiate a well-posed classical initial orbit determination (IOD) problem, such as angles-only IOD. Traditional orbit determination methods rely on the curvature of the measurements in order to produce a state estimate. However, measurements obtained from a short observation or a very short sequence of observations have linear dynamics and traditional methods fail as the observation time decreases.[6] Optical sensors measure state information as either a series of angle measurements over time or from streaks formed during a single observation; these angular measurements form a tracklet, but the range and range-rate of the SO are not observable. Therefore, the SO state is underdetermined and for any given tracklet, a continuum of range and range-rate solutions are possible which define the admissible region for a given observation.[7]

In an operational environment when UCTs cannot be correlated with known objects in the Space Object Catalog (SOC), operators must have a method to quickly determine if a potential threat exists. Extreme examples of potential threats include a decreased capability due to a breakup of an asset, or a debris field created by a collision. These debris objects must have had an origin, and it is currently computationally difficult and time consuming to solve this problem with real-time accuracy, and as a result collisions and fragmentations of smaller space objects have occurred. To accurately correlate new UCTs with a known

*Graduate Researcher, Daniel Guggenheim School of Aerospace Engineering, Georgia Institute of Technology, 270 Ferst Dr. Atlanta, GA 30313.

catalog object's orbit as an origin, multiple orbits must occur for LEO cases, and hours of continuous tracking is required for GEO cases. In this situation, it is more efficient to take a collection of UCTs and propagate them back over a designated period of time to determine if any of the possible states shared the same position at the same epoch, which would indicate that the observed UCTs were disparate debris from a known catalog object. Using admissible regions to initiate this approach allows the tasks of initial orbit determination and tracking to be foregone, which allows for faster actionable information. This would allow operators to track incoming UCTs and assign them as fragments or debris from a past event with a tracked catalog object, and allow for tasking of Space Surveillance Network assets to observe the catalog object as well as characterize the current state and future risks that these debris objects may pose.

Admissible region ($\mathcal{AR}$) methods are methods to constrain undetermined states using a priori constraint hypotheses, and have been proposed to support data association and track-initiation tasks. Many have extended the applicability of AR methods to space situational awareness (SSA) since Milani et. al. first proposed applying these methods to the detection of asteroids too-short arc (TSA) problems.[8] The AR approach has been applied by Tommei et. al. to SO detection and discrimination by using radar and optical measurements.[9] Optimization methods to identify a best-fitting orbit solution are proposed by Siminski et. al.[10] Existing admissible region methods can be used discretizing the admissible region and considering the solutions at discrete points, which would allow for a particle filter approach.[1] Additionally, an optimization scheme can be used to identify the best fitting orbits within and admissible region eliminating the need to discretize the whole region.[10] Fujimoto and Scheeres work shows that observations can be associated by applying Bayes' rule to an admissible region generated from two epochs, where a nonzero result indicates that the observations are correlated.[11] In addition, a solution technique for correlating multiple optical observations by computing the overlap between their admissible regions, as well as using highly constrained probability distributions in Poincare orbit element space has been proposed by Fujimoto and Scheeres by.[12] Worthy et. al. has developed an observation association method which uses an optimization based approach to identify local Mahalonobis distance minima in state space between two uncertain admissible regions.[13] A limitation of these methods using the intersection of the $\mathcal{AR}$ volumes is that a feasible orbit can only be constructed if the observations are the same object, otherwise these iterative solution methods will fail. The proposed methodology in this paper seeks to demonstrate that given multiple new debris objects, that cannot be associated with any known catalog catalog object, determine if a collision or fragmentation event has occurred, and from what origin, in near real-time as new UCTs become available.

This paper proposes a methodology for applying AR methods to bound the feasible orbit solutions of multiple observations using constraints on energy and radius of periapsis, propagating them to a common epoch in the past, and using sequential quadratic programming optimization to find a set of solution states that minimize the Euclidean distance between the observations at that time. This numerical zero-finding approach demonstrates that given two uncorrelated observations, and corresponding admissible regions, a line of feasible solutions exist that minimize the distance between the objects. In summary, this paper demonstrates that from using the hypothesized constraint of the admissible regions it is possible to determine if a combination of new uncorrelated debris objects have a common origin that also intersects with a known catalog object orbit, thus indicating a collision or fragmentation has occurred.

II. Approach and Methodology

The goal of this methodology is to detect collisions and fragmentations by observing disparate debris without requiring the computational and time burden of using orbit determination. This approach can be used for a variety of orbit types and observation lengths. Given two uncorrelated observations, at two different times, t_1 and t_2, the proposed method will determine if a common origin exists for these objects at a selected epoch t_0. Figure 1 shows the orbital path in $\mathbb{R}^6$ orbit element space of a known catalog object as a function of time, until at some t_0 a break-up event occurs that results in a discrete number of debris objects. Each observation at t_1 and t_2 are of different debris from what is hypothesized to be a common origin.

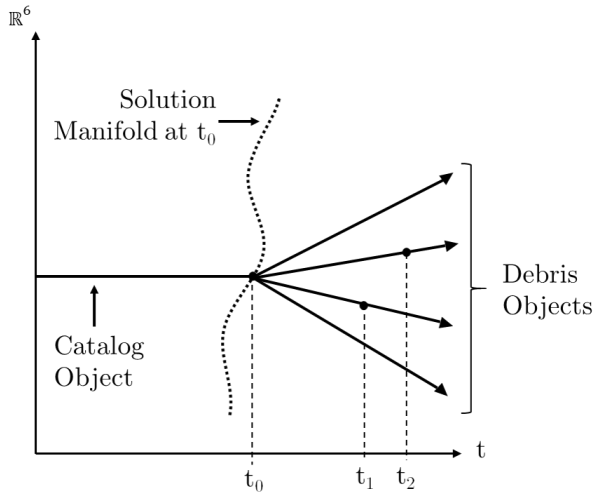

Figure 1. Catalog Object Break-up at a given Epoch as a function of time

Given independent observations of multiple debris objects, a continuum of range and range-rate combinations define the admissible region. These range and range-rate solutions make up the undetermined portion of a potential full state; each full-state (determined or observable information combined with unobservable) correspond to a given position and velocity solution. These solutions can be propagated back to an arbitrary estimated epoch t_0, at which a solution manifold can be constructed by using sequential quadratic programming and selected constraint criteria to minimize the Euclidean distance between the positions of the two observed objects at t_0. The solution manifold represents a line of possible common origins that goes through $\mathbb{R}^6$; if it intersects with the catalog object orbit then the observed have spawned from a break-up event involving that known object. Figure 1 is a three dimensional illustration of the previous figure, but at a particular time. Notice this figure that the solution manifold will cross the orbit of the catalog object at the hypothesized epoch t_0.

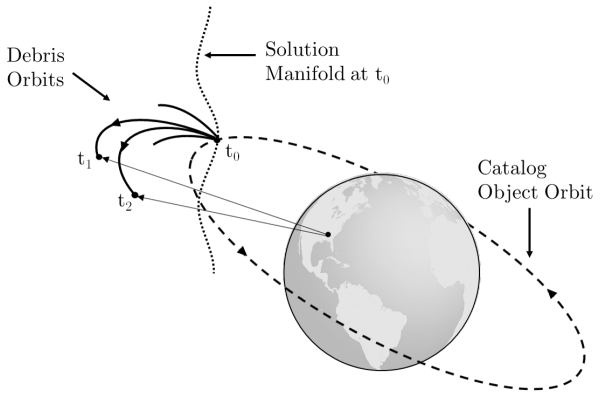

Figure 2. Catalog Object Break-Up and Observation of Debris Objects from Ground Station

Optical measurements generate angle and angle rates of objects tracked using a streak or sequence of angle measurements of right ascension, α, and declination, δ. Te parameters associated with optical measurements include the observer position and velocity, $\mathbf{o}$ and $\dot{\mathbf{o}}$, respectively, as well as the times at which the observations are made. Using this information, the position, $\mathbf{r}$, and velocity, $\mathbf{v}$ of the object are given by

$$\mathbf{r} = \mathbf{o} + \rho\hat{\mathbf{l}} \tag{1}$$

where ρ is the range to the target, $\dot{\rho}$ is the range-rate, and $\hat{\mathbf{l}}$, $\hat{\mathbf{l}}_\alpha$, and $\hat{\mathbf{l}}_\delta$ are given by

$$\mathbf{v} = \dot{\mathbf{o}} + \dot{\rho}\hat{\mathbf{l}} + \rho\dot{\alpha}\hat{\mathbf{l}}_\alpha + \rho\dot{\delta}\hat{\mathbf{l}}_\delta \tag{2}$$

$$\hat{\mathbf{l}} = \begin{bmatrix} cos\alpha cos\delta \\ sin\alpha cos\delta \\ sin\delta \end{bmatrix} \tag{3}$$

$$\hat{\mathbf{l}}_\alpha = \begin{bmatrix} -sin\alpha cos\delta \\ cos\alpha cos\delta \\ 0 \end{bmatrix} \tag{4}$$

$$\hat{\mathbf{l}}_\delta = \begin{bmatrix} -cos\alpha sin\delta \\ -sin\alpha sin\delta \\ cos\delta \end{bmatrix} \tag{5}$$

For this system, the states $\mathbf{x}$, the observations $\mathbf{k}$, and parameters $\mathbf{p}$ are defined as

$$\mathbf{x}^T = \begin{bmatrix} \alpha & \dot{\alpha} & \delta & \dot{\delta} & \rho & \dot{\rho} \end{bmatrix} \tag{6}$$

$$\mathbf{k}^T = \begin{bmatrix} \alpha_1 & \dots & \alpha_q & \delta_1 & \dots & \delta_q \mathbf{o}^T & \dot{\mathbf{o}}^T \end{bmatrix} \tag{7}$$

$$\mathbf{p}^T = \begin{bmatrix} \mathbf{o}^T & \dot{\mathbf{o}}^T \end{bmatrix} \tag{8}$$

where $\dot{\alpha}$ and $\dot{\delta}$ are the angle rates which are generated using Lagrange Interpolation shown in Equation 9, and q is the number of observations. In order to limit the inherent error associated with using Lagrange interpolation from point values, streak observations are used in this methodology. The rate estimations from the center of each streak are used for further calculations as this provides a better estimate of the rate than the beginning of the streak.

$$\begin{aligned} \dot{\alpha}(t) = \alpha(t_1)\frac{(t-t_2)+(t-t_3)+\cdots+(t-t_q)}{(t_1-t_2)(t_1-t_3)\dots(t_1-t_q)} + \alpha(t_2)\frac{(t-t_2)+(t-t_3)+\cdots+(t-t_q)}{(t_2-t_1)(t_2-t_3)\dots(t_2-t_q)} \\ +\cdots+\alpha(t_l)\frac{(t-t_2)+(t-t_3)+\cdots+(t-t_{q-1})}{(t_l-t_1)(t_l-t_3)\dots(t_l-t_{q-1})} \end{aligned} \tag{9}$$

For an observation with two measurements, the combined measurement and parameter vector, $\mathbf{y}^T \in \mathbb{R}^{12}$ is given by

$$\mathbf{y}^T = \begin{bmatrix} \alpha_1 & \alpha_2 & \delta_1 & \delta_2 & t_1 & t_2 & \mathbf{o}^T & \dot{\mathbf{o}}^T \end{bmatrix} \tag{10}$$

Given $\mathbf{y}$ and solving for the angle rates using Equation 9, four of the six states in $\mathbf{x}$ can be observed or determined; these four states, known henceforth as $\mathbf{x}_d$ are shown in Equation 11. The remaining two undetermined states, known as $\mathbf{x}_u$, are given by Equation 12.

$$\mathbf{x}_d = \begin{bmatrix} \alpha \\ \dot{\alpha} \\ \delta \\ \dot{\delta} \end{bmatrix}_{4\times 1} \tag{11}$$

$$\mathbf{x}_u = \begin{bmatrix} \rho \\ \dot{\rho} \end{bmatrix}_{2\times 1} \tag{12}$$

To limit the realm of possible solutions for $\mathbf{x}_u$, constraint hypotheses are imposed on the admissible regions. These constraints can be based on a priori information about the observation (e.g. is the object LEO or GEO), as well as reasonable constraints for objects in orbit around Earth can be imposed. For the

purpose of this paper, the primary assumption is that of 2-body motion, which allows the use of a constraint on the specific orbital energy equation. This constraint, κ requires that the space object is in Earth's orbit, and therefore excludes hyperbolic orbit solutions. To constrain these solutions for $\mathbf{x}_u$, the admissible region set $\mathcal{AR}$ can be defined as $\left\{\mathbf{x}_u \in \mathbb{R}^2 | \epsilon(\mathbf{r}, \dot{\mathbf{v}}) = 0\right\}$, which is the solution to Equation 13.[6] The solutions to this polynomial define the two dimensional boundary of the admissible region.

$$\kappa(\mathbf{x}_u, \mathbf{y}) = 2\varepsilon(\mathbf{r}, \mathbf{v}) = \dot{\rho}^2 + w_1\dot{\rho} + T(\rho) - \frac{2\mu}{\sqrt{S(\rho)}} = 0 \tag{13}$$

Farnocchia, et. al. and Tommei et. al. define $T(\rho)$, $S(\rho)$, and coefficients w_0 through w_5 as Equations 14 and 15[14].[9]

$$T(\rho) = w_2\rho^2 + w_3\rho + w_4, \quad S(\rho) = \rho^2 + w_5\rho + w_0 \tag{14}$$

$$\begin{aligned} w_0 &= \|\mathbf{o}\|^2, & w_1 &= 2\left\langle \dot{\mathbf{o}} \cdot \hat{\mathbf{l}} \right\rangle \\ w_2 &= \dot{\alpha}^2 cos^2\delta + \dot{\delta}^2, & w_3 &= 2\dot{\alpha}\left\langle \dot{\mathbf{o}} \cdot \hat{\mathbf{l}}_\alpha \right\rangle + 2\dot{\delta}\left\langle \dot{\mathbf{o}} \cdot \hat{\mathbf{l}}_\delta \right\rangle \\ w_4 &= \|\dot{\mathbf{o}}\|^2, & w_5 &= 2\left\langle \mathbf{o} \cdot \hat{\mathbf{l}} \right\rangle \end{aligned} \tag{15}$$

To further constrain the realm of possible state solutions, a periapsis radius constraint is used to exclude parabolic and potentially re-entering space objects that will impact the Earth in less than one revolution. For the purpose of this paper, the minimum radius of periapsis r_{min} is set at 6378 km plus h_{atm}, where h_{atm} is 200 km. A form of this constraint, $r_p = a(1-e) \geq r_min$ was proposed by Maruskin et. al.[1] The periapsis constraint $r_{min} - r_p(\rho, \dot{\rho})$ was analytically developed by Farnocchia et. al. to be[14]

$$(r_{min}^2 - \|\mathbf{D}\|^2)\dot{\rho}^2 - P(\rho)\dot{\rho} - U(\rho) + r_{min}^2 T(\rho) - \frac{2r_{min}^2\mu}{\sqrt{S(\rho)}} \leq 0 \tag{16}$$

with

$$P(\rho) = 2\mathbf{D}\cdot\mathbf{E}\rho^2 + 2\mathbf{D}\cdot\mathbf{F}\rho + 2\mathbf{D}\cdot\mathbf{G} - r_{min}^2 w_1 \tag{17}$$

$$U(\rho) = \|\mathbf{E}\|^2\rho^4 + 2\mathbf{E}\cdot\mathbf{F}\rho^3 + (2\mathbf{E}\cdot\mathbf{G} + \|\mathbf{F}\|^2)\rho^2 + 2\mathbf{F}\cdot\mathbf{G}\rho + \|\mathbf{G}\|^2 - 2r_{min}\mu \tag{18}$$

given the following

$$\begin{aligned} \mathbf{D} &= \mathbf{o} \times \hat{\mathbf{l}}, & \mathbf{E} &= \hat{\mathbf{l}} \times (\dot{\alpha}\mathbf{l}_\alpha + \dot{\delta}\mathbf{l}_\delta) \\ \mathbf{F} &= \mathbf{o} \times (\dot{\alpha}\mathbf{l}_\alpha + \dot{\delta}\mathbf{l}_\delta) + \mathbf{l} \times \dot{\mathbf{o}}, & \mathbf{G} &= \mathbf{o} \times \dot{\mathbf{o}} \end{aligned} \tag{19}$$

Additional constraints may be relevant depending on available a priori information about the space object. For example, eccentricity would be an appropriate constraint to apply to GEO observations.[1] For the purpose of this paper, only energy and radius of periapsis constraints will be imposed. Imposing these constraints on an observation $\mathbf{y}$ results in a two dimensional space of solutions to $\mathbf{x}_u$ that could possibly complete the state $\mathbf{x}$ of the observed space object.

Given two observations of an object, such as shown in Equation 10, admissible regions can be determined for each observation, $\mathcal{AR}_1$ and AR_2. Each of these have a set of possible undermined states $\mathbf{x}_u$ that satisfy the aforementioned constraints. By combining these into a single variable, into a single variable $\mathbf{z}$

$$\mathbf{z} = \begin{bmatrix} \mathbf{x}_{u,1} \\ \mathbf{x}_{u,2} \end{bmatrix} = \begin{bmatrix} \rho_1 \\ \dot{\rho}_1 \\ \rho_2 \\ \dot{\rho}_2 \end{bmatrix} \tag{20}$$

It is possible to conduct a random uniform sampling of both $\mathcal{AR}_1$ and $\mathcal{AR}_2$ to collect a set of $\mathbf{z}$ solutions that satisfy the constraints. Each $\mathbf{x}_{u,1}$ and $\mathbf{x}_{u,2}$, combined with $\mathbf{x}_{d,1}$ and $\mathbf{x}_{d,2}$, respectively, create a possible full state solution $mathbfx_1$ and$mathbfx_2$ for the observed space object. Each of these states can be converted into Cartesian position $\mathbf{r}$ and velocity $\mathbf{v}$ by using Equations 1 and 2. Propagating these states back to some common time t in the past, the resulting vectors are defined as

$$\begin{aligned}\mathbf{r}_1(t) &= \begin{bmatrix}\mathbb{I} & 0\end{bmatrix}\phi(t, \mathbf{x}_{u,1}, \mathbf{x}_{d,1}, t_1)\\ \mathbf{r}_2(t) &= \begin{bmatrix}\mathbb{I} & 0\end{bmatrix}\phi(t, \mathbf{x}_{u,2}, \mathbf{x}_{d,2}, t_2)\end{aligned} \tag{21}$$

From this, the goal is to determine if there is a set of solutions for $\mathbf{z}$ that minimize the Euclidean distance between the position vectors corresponding to each observation time. The cost function $J(\mathbf{z})$ and gradient are as follows

$$J(\mathbf{z}) = \frac{1}{2}(\mathbf{r}_1 - \mathbf{r}_2)^T(\mathbf{r}_1 - \mathbf{r}_2) \tag{22}$$

$$\frac{\partial J}{\partial \mathbf{z}} = \left[\frac{\partial J}{\partial \mathbf{x}_{u,1}},\ \frac{\partial J}{\partial \mathbf{x}_{u,2}}\right] = \left[(\mathbf{r}_1 - \mathbf{r}_2)^T \cdot \begin{bmatrix}\mathbb{I} & 0\end{bmatrix}\frac{\partial \phi}{\partial \mathbf{x}_1}\frac{\partial \mathbf{x}_1}{\partial \mathbf{x}_{u,1}},\ (\mathbf{r}_1 - \mathbf{r}_2)^T \cdot \begin{bmatrix}\mathbb{I} & 0\end{bmatrix}\frac{\partial \phi}{\partial \mathbf{x}_2}\frac{\partial \mathbf{x}_2}{\partial \mathbf{x}_{u,2}}\right] \tag{23}$$

Algorithm 1: Algorithm to Determine Solution Manifold

Result: Minimize Eq. 22
initialization of givens, observables, and parameter settings;
compute GS Vectors and observer unit vectors with Eq. 3, 4, & 5;
compute $\mathcal{R}$ boundaries for each Obs. by solving the quadratic equation for $\dot{\rho}$ given a continuous set of ρ values using Eq. 13;
uniformly sample from $\mathcal{R}$ interiors by selecting a random ρ & $\dot{\rho}$ based on the min and max values and satisfying the energy (Eq. 13) and radius of periapsis constraints (Eq. 16);
construct $\mathbf{z}$ (Eq. 20) by stacking the sample values from $\mathcal{R}_1$ & $\mathcal{R}_2$;
for *i = 1:length(***z***)* **do**
  Establish current $\mathbf{z}$ "guess" value ($\mathbf{z} = z(:, i)$) ;
  while $J(\tilde{\mathbf{z}}) \geq$ *Tolerance* **do**
    Use fmincon to estimate the gradient (Eq. 23) and step $\mathbf{z}$ in that direction using nonlinear constraints in Eqs. 13 & 16;
    Update $\mathbf{z}$ value to reflect step towards minimum;
    Evaluate constraints (Eq. 13 and Eq. 16) given current $\mathbf{z}$ value to ensure solution still falls within $\mathcal{R}$;
    if *current* $\mathbf{z}$ *not within* $\mathcal{R}$ *(does not meet constraints);*
    then
      Get new "guess" for $\mathbf{z}$ from fmincon by continuing;
    else
      Convert $\mathbf{z}$ to cartesian using Eq. 1 & 2 to get $\tilde{\mathbf{z}}$;
      Propagate $\tilde{\mathbf{z}}$ to t_0 and calculate distance using Eq. 22;
    end
  end
  save $\mathbf{z}$ solution value that minimize $J(\mathbf{z})$ (Eq. 22)
end

III. Results

The goal of this methodology is to detect collisions and fragmentations by observing disparate debris. To demonstrate the initial effectiveness of this approach, two independent optical observations of the same object where used. The observations were made for one second exposures 5 minutes (300 seconds) apart based on an observation taken March 1, 2014 at 02:01:36 UTC. The measurement values for the tested LEO case are given in Table 1.The observations were made using an equatorial mounted telescope from Deerlick Astronomy Village, the observer parameters are given in Table 2. Error in observation measurements were assumed to have a zero angle mean noise and approximately 0.5 arcsecond standard deviation of the noise on the angle observations (right ascension and declination).The standard deviation is approximated at this value due to the type of mount the observations were made from, as well as the exposure time.

Table 1. LEO Optical Observation Measurements

Time	α (rad)	δ (rad)	Exposure (sec)
02:01:36	1.4007	0.5556	1
02:06:36	1.3504	-0.6931	1

Table 2. Observer Parameters for Deerlick Astronomy Village, GA

Latitude	Longitude	Altitude (m)
33.561deg N	82.764deg W	176.8

From these observations, admissible regions were constructed using a radius of periapsis constraint of 6578 km (radius of Earth plus 200km), an energy constraint of less than zero (Earth orbiting), and eccentricity constraint of less than 0.7. A set n particle pairs $\mathbf{x}_u$'s that meet these constraints were then created by randomly uniformly sampling the interiors of each admissible region. Then set from the observation at t_1, $\mathbf{x}_{u,1}$, is combined with $\mathbf{x}_{u,2}$ from the observation at t_2, it results in $\mathbf{z}$ being a $4 \times n$ matrix (Equation 20). Figure 3 shows the admissible regions corresponding to each observation as well as the sampled points from each interior.

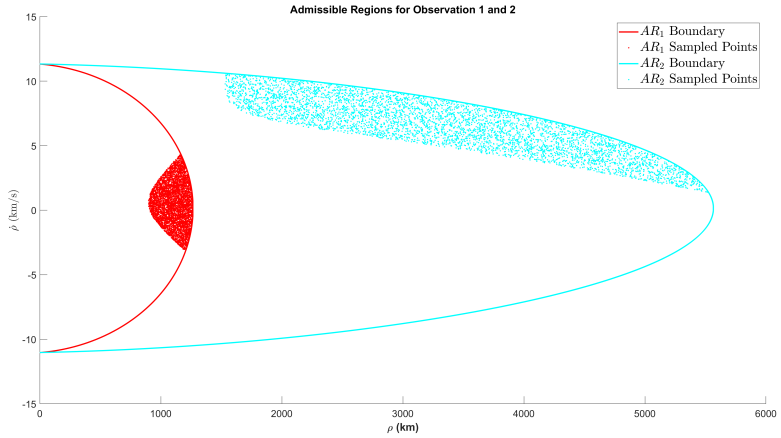

Figure 3. Admissible Region boundaries for Observation 1 & 2

Using this test case, two different epoch times were selected: 100 seconds and 1 hour (3600 seconds) in the past. In each of these scenarios, each column in $mathbfz$ is then stepped towards a minimum solution for the cost function $J(\mathbf{z})$ at time t_0 by using the MATLAB function fmincon from the optimization toolbox to solve for the minimum of Equation 22 given the nonlinear constraints and functions. Fmincon is a gradient-based method that is designed to work on problems where the objective and constraint functions are both continuous and have continuous first derivatives.

A. Epoch Time = -100 Seconds

In this scenario, 5000 particles were sampled from the admissible regions, resulting in a 4×5000 matrix for $\mathbf{z}$. Each of the 5000 columns of $\mathbf{z}$ was propagated backwards 100 seconds using a two-body propagator in Ode45. The solution values for $\mathbf{z}$, that correspond to each observation, that minimize the Euclidean distance between the observed objects are shown in Figures 4 and 5. At an epoch that is only 100 seconds before the first observation, the solution manifold appears to have very limited curvature.

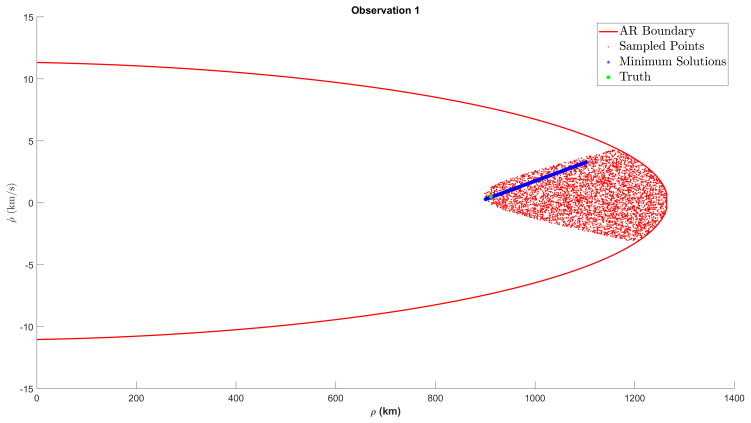

Figure 4. Admissible Region for Observation 1 with minimized solutions and truth for $t_0 = -100sec$

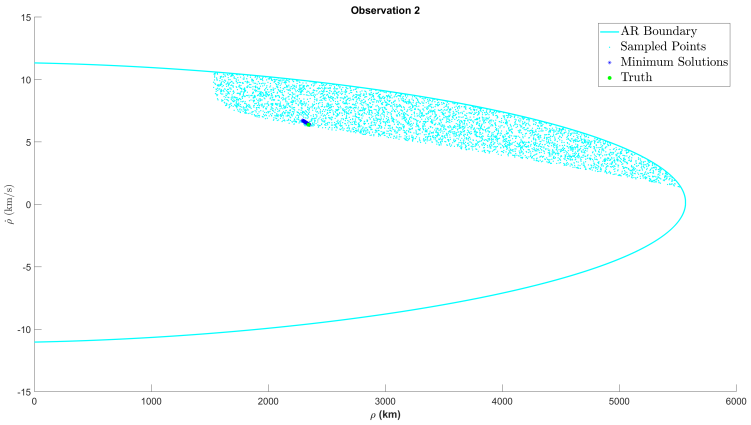

Figure 5. Admissible Region for Observation 2 with minimized solutions and truth for $t_0 = -100sec$

The solution manifold line in the first observation's admissible region is much longer than the corresponding line in the second observation's admissible region. This result was to be expected, as the first observation was taken at a minimum range to the ground station, which means that a set of possible solution orbits with larger variation are possible. Conversely, the second observation was taken at a much lower elevation, thus increasing the slant range to the object from the ground station. This provides a smaller amount of variation in the solution states. The 3D plots shown in Figures 6 and 7 show the solution manifold in the position and velocity space. In these figures, the first observation is indicated with a blue arrow, the second with an orange arrow, and the ground station with a green arrow. The solution manifold is a short line made up of red (observation 1) and blue (observation 2) position solutions that clearly intersects with the shown known object truth orbit at the given epoch. This indicates that the observed debris objects have the same origin and it is possible that they spawned from an event involving the shown known object orbit.

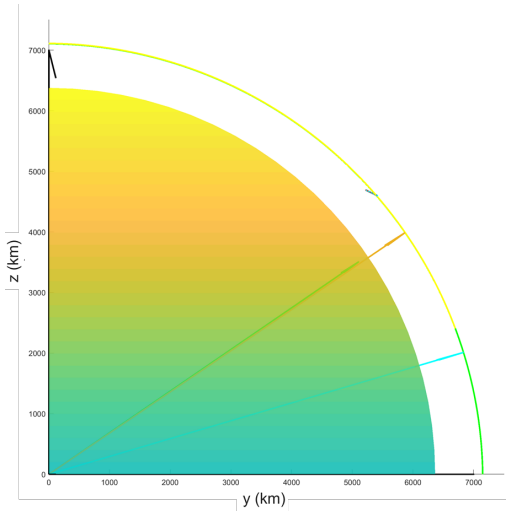

Figure 6. 3D Plot Earth Hemisphere with Solution Manifold and True Catalog Orbit for $t_0 = -100sec$

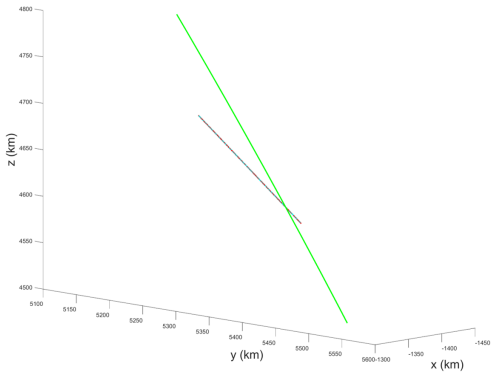

Figure 7. Solution Manifold and True Catalog Orbit Intersection for $t_0 = -100sec$

B. Epoch Time = -1 Hour

In this scenario, 1100 particles were sampled from the admissible regions, resulting in a 4×1100 matrix for **z**. Each of the 1100 columns of $mathbfz$ was propagated backwards one hour (3600 seconds) using a two-body propagator in Ode45. The solution values for $mathbfz$, that correspond to each observation, that minimize the Euclidean distance between the observed objects are shown in Figures 4 and 5. At an epoch that is one hour prior to the first observation, the solution manifold appears to have an increased amount of curvature when compared with the corresponding results form the previous scenario. This is especially true of the solution manifold in Observation 2's admissible region.

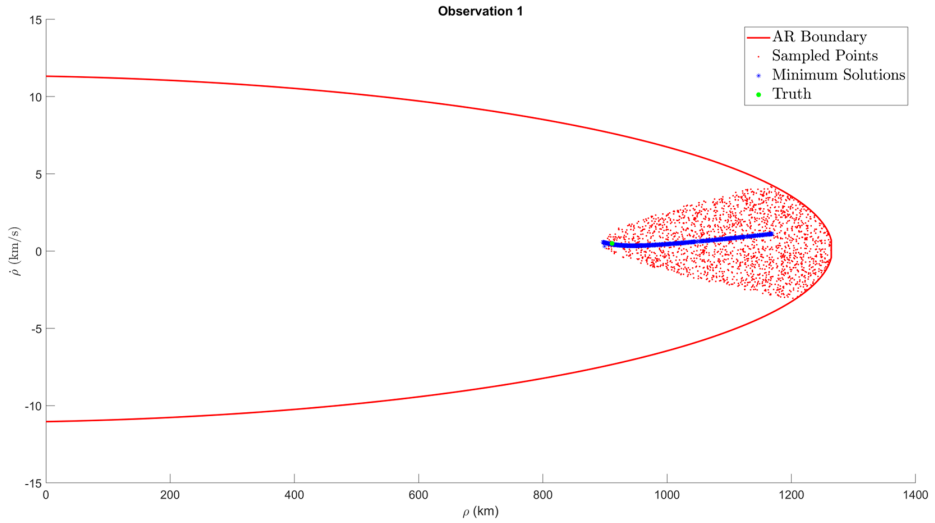

Figure 8. Admissible Region for Observation 1 with minimized solutions and truth for $t_0 = -3600sec$

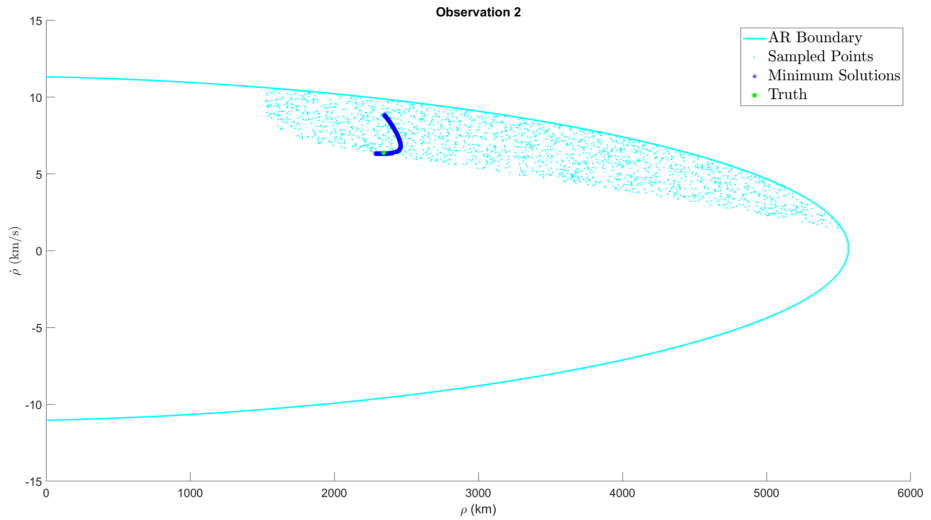

Figure 9. Admissible Region for Observation 2 with minimized solutions and truth for $t_0 = -3600sec$

Just as was shown with the first scenario, the solution manifold line in the first observation's admissible region is much longer than the corresponding line in the second observation's admissible region. However, for an epoch of one hour prior to the first observation, the solution manifolds display much more curvature than the 100 second scenario. This is especially evident in the solution manifold corresponding to observation 2 in Figure 9. The 3D plots shown in Figure 10 show the solution manifold in the position and velocity space. In this figure, the first observation is indicated with a blue arrow, the second with an orange arrow, and the ground station with a green arrow. The solution manifold is a short line made up of red (observation 1) and blue (observation 2) position solutions that clearly intersects with the shown known object truth orbit at the given epoch. This indicates that the observed debris objects have the same origin and it is possible that they spawned from an event involving the shown known object orbit. The solution manifold displays much more interesting characteristics and curvature in this scenario, as it extends well beyond the known object orbit.

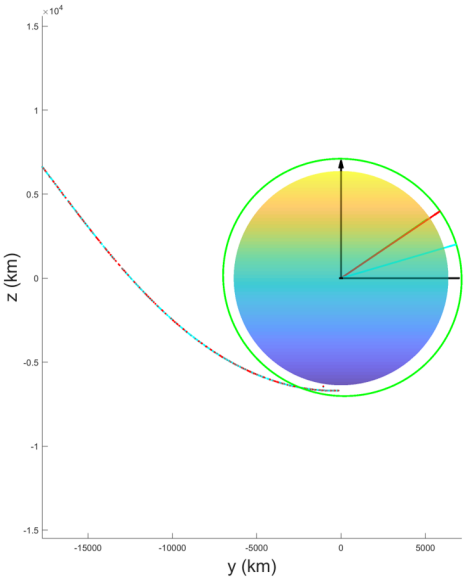

Figure 10. 3D Plot Earth Hemisphere with Solution Manifold and True Catalog Orbit for $t_0 = -3600sec$

C. Error and Challenges

Error in observation measurements were assumed to have a zero angle mean noise and approximately 0.5 arcsecond standard deviation of the noise on the angle observations (right ascension and declination). The standard deviation is approximated at this value due to the type of mount the observations were made from, as well as the exposure time. Error also is inherrent with any numerical propagation method, such as Ode45. The relative and absolute tolerances were set to $1e^{-12}$ to limit error throughout this process. Additional sources of error can be found from using Lagrangian interpolation in order to estimate the angle rates of each observation. As aforementioned, to minimize this error source, streaks were used and the observation information from the center of the streak was used and the rates were estimated using the beginning and the end of the streak. For future work, the rates will be fed in as part of the 4-state $\mathbf{x}_d$ and not estimated based on the right ascension and declination of the observations. This approach is computationally slow because implementing fmincon, which estimates the gradient, instead of using a gradient based approach like steepest descent. A limitation of the method described here is that the epoch time, t_0 is arbitrary, and may be based on a priori information (e.g. last known observation, etc.), but would require an iterative "guessing" process to select a good estimate for t_0 which increases computational cost.

IV. Conclusions

The results in this paper, though there are limitations, illustrate that it is possible to detect fragmentations and collisions much sooner than current capabilities that rely on orbit determination. The current state-of-the-art relies on orbit determination, which requires multiple observations over at least two orbits for a LEO object and continual observation over hours for a GEO object. The approach outlined in this paper requires only independent observations of two debris orbits and to answer the same hypothesis, with the cost largely in computation. The problem reduces to a 4-dimensional particle swarm optimization, which can easily be solved using a gradient-based method. By using the hypothesized constraint of the admissible regions it was demonstrated that it is possible to determine if a combination of new uncorrelated debris objects have a common origin that also intersects with a known catalog object orbit, thus indicating break-up of that known object has occurred.

V. Future Work

This paper reflects a very initial endeavour into understanding the limitations and applications of this methodology. Additional test cases, including one on a GEO break up as well as another using LEO collision path, will need to be done, as this paper only demonstrates that if you have two observations of the same object that that a zero-finding problem is possible. Other phenomonenology should also be considered, such as radar observations. LEO observations are not typically made using optical or electro-optical hardware; conversely, GEO observations are almost exclusively made with these methods. Radar observations have different admissible region structure, as they provide a different set of observable, or determined states. In this scenario, $\mathbf{x}_d$ is a 2×1 matrix, whereas in optical it is 4×1 matrix. Therefore, to use radar information in the methodology described in this paper, additional observations would need to be included to create a closed solution.

References

[1]J. M. Maruskin, D. J. Scheeres, and K. T. Alfriend, "Correlation of optical observations of objects in earth orbit," *Journal of Guidance, Control, and Dynamics*, Vol. 32, No. 1, 2009, pp. 194–209.

[2]A. Rossi, "The earth orbiting space debris," *Serbian Astronomical Journal*, Vol. 170, 2005, pp. 1–12.

[3]M. J. Holzinger, K. K. Luu, C. Sabol, and K. Hill, "Uncorrelated-Track Classification, Characterization, and Prioritization Using Admissible Regions and Bayesian Inference," *Journal of Guidance, Control, and Dynamics*, 2016, pp. 2469–2484.

[4]K. Wormnes, R. Le Letty, L. Summerer, R. Schonenborg, O. Dubois-Matra, E. Luraschi, A. Cropp, H. Krag, and J. Delaval, "ESA technologies for space debris remediation," *6th IAASS Conference:Safety is Not an Option, Montrel*, 2013.

[5]P. d. Selding, "Orbital Debris a Growing Problem with No End in Sight," *Space News*, Vol. 31, 2006.

[6]J. L. Worthy, *Initialization of sequential estimation for unobservable dynamical systems using partial information in the presence of systemic uncertainty.* PhD thesis, Georgia Institute of Technology, 2017.

[7]J. L. Worthy III and M. J. Holzinger, "Incorporating uncertainty in admissible regions for uncorrelated detections," *Journal of Guidance, Control, and Dynamics*, Vol. 38, No. 9, 2015, pp. 1673–1689.

[8]A. Milani, G. F. Gronchi, M. d. Vitturi, and Z. Knežević, "Orbit determination with very short arcs. I admissible regions," *Celestial Mechanics and Dynamical Astronomy*, Vol. 90, No. 1-2, 2004, pp. 57–85.

[9]G. Tommei, A. Milani, and A. Rossi, "Orbit determination of space debris: admissible regions," *Celestial Mechanics and Dynamical Astronomy*, Vol. 97, No. 4, 2007, pp. 289–304.

[10]J. A. Siminski, O. Montenbruck, H. Fiedler, and T. Schildknecht, "Short-arc tracklet association for geostationary objects," *Advances in space research*, Vol. 53, No. 8, 2014, pp. 1184–1194.

[11]K. Fujimoto and D. J. Scheeres, "Applications of the admissible region to space-based observations," *Advances in Space Research*, Vol. 52, No. 4, 2013, pp. 696–704.

[12]K. Fujimoto and D. J. Scheeres, "Correlation of optical observations of earth-orbiting objects and initial orbit determination," *Journal of guidance, control, and dynamics*, Vol. 35, No. 1, 2012, pp. 208–221.

[13]J. L. Worthy, M. J. Holzinger, and D. J. Scheeres, "An optimization approach for observation association with systemic uncertainty applied to electro-optical systems," *Advances in Space Research*, 2018.

[14]D. Farnocchia, G. Tommei, A. Milani, and A. Rossi, "Innovative methods of correlation and orbit determination for space debris," *Celestial Mechanics and Dynamical Astronomy*, Vol. 107, No. 1-2, 2010, pp. 169–185.